

Anisotropic behaviors of massless Dirac fermions in graphene under periodic potential

Cheol-Hwan Park,^{1,2} Li Yang,^{1,2} Young-Woo Son,³ Marvin L. Cohen,^{1,2} and Steven G. Louie^{1,2}

¹*Department of Physics, University of California at Berkeley, Berkeley, California 94720, USA*

²*Materials Sciences Division, Lawrence Berkeley National Laboratory, Berkeley, California 94720, USA*

³*Department of Physics, Konkuk University, Seoul 143-701, Korea*

(Dated: submitted, October 2, 2007)

Charge carriers of graphene show neutrino-like linear energy dispersions as well as chiral behavior near the Dirac point^{1,2,3,4,5,6}. Here we report highly unusual and unexpected behaviors of these carriers in applied external periodic potentials, i.e., in graphene superlattices. The group velocity renormalizes highly anisotropically even to a degree that it is not changed at all for states with wavevector in one direction but is reduced to zero in another, implying the possibility that one can make nanoscale electronic circuits out of graphene not by cutting it^{7,8,9,10} but by drawing on it in a non-destructive way. Also, the type of charge carrier species (e.g. electron, hole or open orbit) and their density of states vary drastically with the Fermi energy, enabling one to tune the Fermi surface-dominant properties significantly with gate voltage. These results address the fundamental question of how chiral massless Dirac fermions propagate in periodic potentials and point to a new possible path for nanoscale electronics.

Since the pioneering work by Esaki and Tsu¹¹, superlattices have been studied extensively and have had a huge impact on semiconductor physics^{12,13}. Superlattices demonstrate interesting phenomena such as negative differential conductivity, Bloch oscillations, gap openings at the mini Brillouin zone boundary formed by the additional periodic potential, etc^{12,13}. Conventional semiconducting superlattices are mainly produced by molecular-beam epitaxy and metallo-organic chemical vapour-phase deposition while metallic superlattices are made by sputtering procedures^{12,13}. We expect that, by modulating the potential seen by the electrons, graphene superlattices may be fabricated by adsorbing adatoms on graphene surface through similar techniques, by positioning and aligning impurities with scanning tunneling microscopy^{14,15,16}, or by applying a local top-gate voltage to graphene^{17,18,19}. Epitaxial growth of graphene⁵ on top of pre-patterned substrate is also a possible route to graphene superlattice. Recently, periodic pattern in the scanning tunneling microscope image has been demonstrated on a graphene monolayer on top of a metallic substrate^{20,21,22} as well.

The low energy charge carriers in pristine graphene are described by a massless Dirac equation and have a linear energy dispersion which is isotropic near the Dirac points K and K' in the Brillouin zone^{1,3,4,23,24,25} (Fig. 1a). It is shown experimentally that the carriers have a group ve-

locity of $v_0 \approx 10^6$ m/s which plays the role of an effective speed of light in (2+1) dimensional quantum electrodynamics^{3,4}. Within the effective-Hamiltonian approximation,

$$H = \hbar v_0 \begin{pmatrix} 0 & -ik_x - k_y \\ ik_x - k_y & 0 \end{pmatrix},$$

where k_x and k_y are the x and y components of the wavevector \mathbf{k} of the Bloch state defined with respect to the Dirac point, the wavefunction of the quasiparticles in graphene has two components corresponding to the amplitude on the two different trigonal sublattices of graphene and can be represented by a two component spinor^{23,24,25}. This spinor structure of the wavefunction is called a pseudospin (because it is not related to a real spin) or chirality^{23,24,25,26,27}, which is of central importance to the novel physical properties of graphene superlattices discussed below.

Let us now consider the situation that an additional periodic potential is applied to graphene. If the spatial period of the superlattice potential is much larger than the nearest neighbor carbon-carbon distance in graphene (~ 1.42 Å), the scattering of a state close to one Dirac point to another one does not occur^{23,24,26}. Therefore, even though there are two nonequivalent Dirac cones for the energy dispersion surface of graphene, focusing on a single cone is sufficient. This condition also implies that, in the graphene superlattices discussed here, there is no gap opening at the Dirac point^{23,24,26}.

To investigate the physics of charge carriers in graphene superlattices, we have calculated the energy dispersions, the group velocities, and energy gap openings at the minizone boundaries (MB) within the effective-Hamiltonian formalism¹. Effects of the external periodic potential are incorporated into our calculation through the scattering matrix elements between pseudospin states, or chiral eigenstates, of the electrons in graphene:

$$\langle s, \mathbf{k} | U(\mathbf{r}) | s', \mathbf{k}' \rangle = \sum_{\mathbf{G}} \frac{1}{2} (1 + ss' e^{-i\theta_{\mathbf{k}, \mathbf{k}-\mathbf{G}}}) U(\mathbf{G}) \delta_{\mathbf{k}', \mathbf{k}-\mathbf{G}}.$$

Here, \mathbf{G} 's are reciprocal lattice vectors of the superlattice and $\theta_{\mathbf{k}, \mathbf{k}-\mathbf{G}}$ is the angle between \mathbf{k} and $\mathbf{k}-\mathbf{G}$. $U(\mathbf{r})$ and $U(\mathbf{G})$ are external potential in real and wavevector space, respectively. s and s' are either +1 or -1 depending on whether the energy of the state is above or below the energy at the Dirac point, respectively. We have also carried out a tight-binding formulation and obtained identical results as those discussed below.

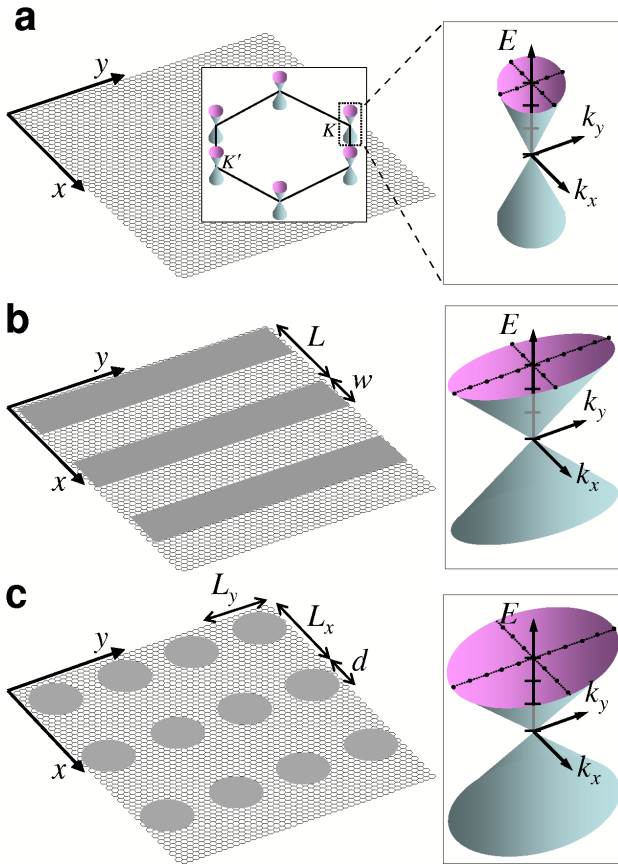


FIG. 1: **Graphene superlattices and anisotropic Dirac cones.** **a**, Schematic diagram of graphene. Inset: the Brillouin zone of graphene and Dirac cones centered at Dirac points among which two (K and K') are nonequivalent (left) and the linear and isotropic energy dispersion near one of the Dirac points of charge carriers in graphene (right). **b**, One-dimensional (1D) graphene superlattice formed by Kronig-Penney type of potential periodic along \hat{x} direction with spatial period L and barrier width w . The potential is U_{1D} in the grey regions and zero outside. Inset: energy dispersion of charge carriers in 1D graphene superlattice. The energy dispersion along any line in two-dimensional (2D) wavevector space from the Dirac point is linear but with different group velocity. For a particle moving parallel to the periodic direction, the group velocity (v_{\parallel}) is not renormalized at all whereas that for a particle moving perpendicular to the periodic direction (v_{\perp}) it is reduced most. **c**, 2D graphene superlattice with muffin-tin type of potential periodic along both \hat{x} and \hat{y} directions with spatial periods L_x and L_y , respectively. The potential is U_{2D} inside the grey disks with diameter d and zero outside. Inset: energy dispersions of charge carriers in 2D graphene superlattice.

First, for a one-dimensional (1D) graphene superlattice (Fig. 1b), we find that the group velocity for states with wavevector \mathbf{k} (\mathbf{k} is the wavevector of the Bloch state defined with respect to the Dirac point), is anisotropically renormalized, i.e., it is a strong function of the direction of \mathbf{k} . For pristine graphene, the group velocity of states near the Dirac point is parallel to \mathbf{k} and of constant mag-

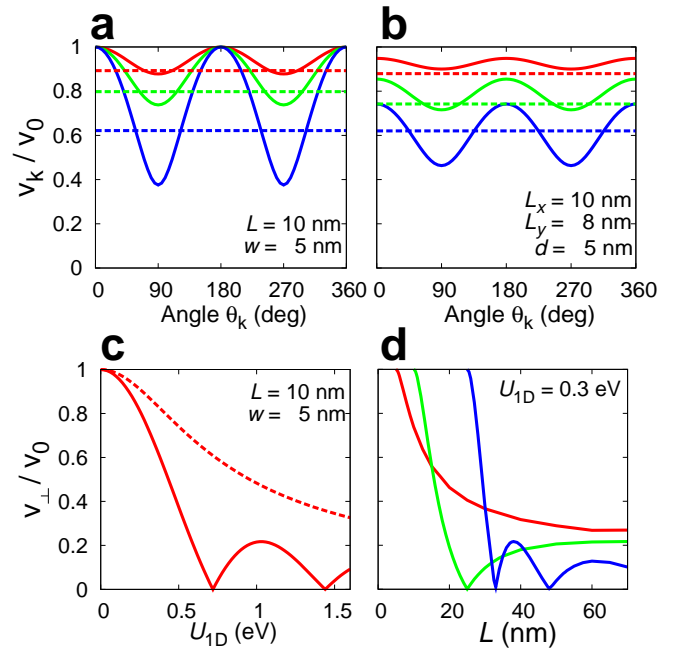


FIG. 2: **Anisotropic velocity renormalization in graphene superlattices.** **a**, The component of the group velocity parallel to the \mathbf{k} vector [$v_k \equiv \mathbf{v}(\mathbf{k}) \cdot \hat{k}$ with \mathbf{k} measured from the Dirac point] of charge carriers in a 1D graphene superlattice in units of the Fermi velocity in graphene (v_0) versus the angle (θ_k) of the \mathbf{k} -vector from the periodic potential direction \hat{x} (solid lines) and that in a superlattice made from a fictitious system of nonchiral fermions with properties otherwise identical to those in graphene (dashed lines). Red, green and blue lines correspond to U_{1D} being 0.2 eV, 0.3 eV and 0.5 eV, respectively. **b**, Similar quantities as in **a** for a rectangular 2D graphene superlattice. Red, green and blue lines correspond to U_{2D} being 0.3 eV, 0.5 eV and 0.7 eV, respectively. **c**, The group velocity of charge carriers in a 1D graphene superlattice (solid line) with \mathbf{k} perpendicular to the periodic direction, v_{\perp} , in units of v_0 versus U_{1D} (solid line) and that in a superlattice made from a fictitious system of nonchiral fermions with properties otherwise identical to those in graphene (dashed line). **d**, v_{\perp} versus the potential spatial period (L) of charge carriers in a 1D graphene superlattice. Red, green and blue lines correspond to a fixed potential barrier height but with width (w) being 5 nm, 10 nm and 25 nm, respectively.

nitude (v_0). For example, in a 1D superlattice of Kronig-Penney type of periodic potential with potential barrier height (U_{1D}) of 0.5 eV and spatial period (L) and barrier width (w) of 10 nm and 5 nm, respectively, the group velocity of the charge carriers when \mathbf{k} is along certain direction is renormalized to be slower than 40 % of its original value v_0 but is the same as v_0 along some other direction. [Fig. 2a: the plotted quantity $v_k \equiv \mathbf{v}(\mathbf{k}) \cdot \hat{k}$ is the component of the group velocity parallel to the wavevector \mathbf{k} in units of v_0 . We note that this quantity which depends only on the direction of \mathbf{k} (Supplementary Discussion 2) is exactly equal to the absolute value of the group velocity v_g when \mathbf{k} is at 0, 90, 180 or 270 degrees

from the periodic direction of the applied potential and, when the applied potential is weak, is only slightly different from v_g at other angles (Supplementary Discussion 3.) Thus, the group velocity of charge carriers can be tailored highly anisotropically in graphene superlattices. More interestingly, the group velocity when \mathbf{k} is along the direction perpendicular to the periodic direction of the potential (v_{\perp}) is reduced the most, whereas when \mathbf{k} is in the parallel direction, it is not renormalized at all (Fig. 1b). This result is counter-intuitive since the velocity is strongly reduced when the charge carrier is moving parallel to the hurdles, but is not modulated when it is crossing them.

To understand the physics behind this phenomenon, we have performed the same calculation for a fictitious system with carriers that have no chirality but otherwise identical to those in graphene including the linear energy dispersion. The group velocity in this system is reduced isotropically and the renormalized group velocity is close to v_{\perp} , i.e., the maximally renormalized one, in 1D graphene superlattices (Fig. 2a). Thus, it is clear that the absence of velocity renormalization in the direction parallel to the periodicity of the external potential originates from the chiral nature of the electronic states of graphene. This behavior can be demonstrated more clearly by second order perturbation theory in the case of the 1D periodic potential with weak amplitudes (Supplementary Discussion 2). We note that the chirality discussed here is also important in tunneling phenomenon in graphene through a single barrier²⁷ or a finite number of barriers²⁸.

In the case of two-dimensional (2D) graphene superlattices, the group velocity is renormalized for \mathbf{k} states along every direction, but anisotropically (Fig. 1c). As the amplitude of the potential increases the overall group velocity is reduced and the ratio of the maximum group velocity to the minimum one is enhanced (Fig. 2b). Here, again, the anisotropy disappears if the chiral nature of the states in graphene is arbitrarily removed. As was demonstrated for the 1D superlattice, the sinusoidal dependence on the angle of propagation as well as the overall shift in the case of 2D graphene superlattice of the component of the renormalized group velocity parallel to \mathbf{k} in the weak potential limit is well explained and reproduced by second order perturbation theory (Supplementary Discussion 2).

Remarkably, the anisotropy in energy dispersions of the 1D superlattices can be tuned by changing the applied potential in such a way that v_{\perp} is reduced completely to zero (Fig. 2c). Hence, we can achieve extremely low mobility in one direction and normal conduction in another one simultaneously. This enables one to control the flow of electrons dramatically. It also provides a novel non-destructive pathway to make graphene nanoribbons^{7,8,9,10} which have been actively pursued by way of cutting graphene sheets^{9,10}. The chiral nature of the states in graphene also plays a decisive role here. In the model without chirality as discussed before the

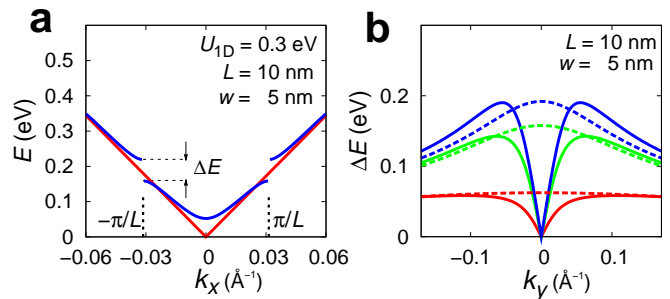


FIG. 3: Energy gap at the superlattice Brillouin zone or minizone boundary of a 1D graphene superlattice. **a**, Energy of charge carriers in 1D graphene superlattice versus the component of the wavevector \mathbf{k} parallel to the periodic potential direction (k_x) at a fixed k_y . Dashed vertical lines indicate minizone boundaries ($k_x = \pm\pi/L$). ΔE is the energy gap at the minizone boundary for a given k_y . Red and blue lines correspond to k_y being zero and 0.012 \AA^{-1} , respectively. **b**, ΔE versus k_y for charge carriers in 1D graphene superlattice (solid lines) and that in a superlattice made from a fictitious system with states without chirality but otherwise identical to graphene (dashed lines). Red, green and blue lines correspond to U_{1D} being 0.1 eV, 0.3 eV and 0.5 eV, respectively.

(isotropic) group velocity of charge carriers is reduced monotonically and never reaches zero within a conceivable range of the potential amplitude (Fig. 2c). We can also achieve vanishing group velocity in one direction by changing the length parameters of the superlattice (Fig. 2d).

Graphene superlattices show peculiar behavior of gap openings at the MB formed by the external periodic potential (Fig. 3). In conventional layer-structured 1D superlattices, gap opening at the MBs is considered to be nearly constant, independent of \mathbf{k} . 1D graphene superlattices, however, are different in that the gap (ΔE) vanishes when \mathbf{k} is along the direction of the periodic potential, i.e., at the centre of the MB (Fig. 3a and 4a). Moreover, the size of the gap depends strongly on where it is on the MB (Fig. 3b). These strong anisotropies in the gap opening do not happen in superlattices made from a system having linear energy dispersions but no chirality (Fig. 3b). Hence, again, the chiral nature of charge carriers in graphene is key in generating these anisotropies in the gap opening as it does in the velocity renormalization. In particular, the gap closure at the centre of the MB is directly related to the absence of back-scattering of charge carriers from a scattering potential when the size of the scatterer is several times larger than the inter-carbon distance^{23,24,26}. In 1D graphene superlattices, the important length-scale is L , which is much larger than the inter-carbon distance, and hence the gap does not open at the centre of the MB.

The largest gap at the MB in a graphene superlattice is proportional to the amplitude of the applied potential if the potential is weak (i.e., small compared to the band width) and the size of which thus can be made to be a few

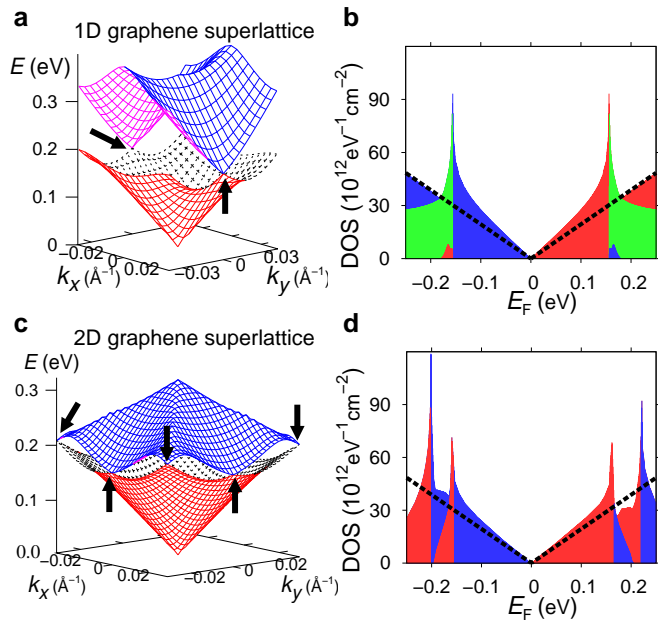


FIG. 4: Energy dispersions and densities of states of charge carriers in graphene superlattices. **a**, Energy of charge carriers in 1D graphene superlattice with $U_{1D} = 0.3$ eV, $L = 10$ nm and $w = 5$ nm in the first (red and black) and the second (blue and pink) band above the vertex of the Dirac cone versus 2D wavevector \mathbf{k} away from the Dirac point. Minizone boundaries are at $k_x = \pm 0.031$ \AA^{-1} . Arrows indicate points on the minizone boundary where the gap closes. **b**, Density of states (DOS) of charge carriers in electron orbits (red), open orbits (green) and hole orbits (blue) in the 1D graphene superlattice characterized in **a** versus the Fermi energy (E_F). The origin of the energy scale is set at the energy of the Dirac point. The DOS of each species is the height of the corresponding colored region. Dashed black line shows the DOS of pristine graphene for comparison. **c**, Similar quantities as in **a** for a 2D graphene superlattice with $U_{2D} = 0.3$ eV, $L_x = L_y = 10$ nm and $d = 5$ nm. **d**, Similar quantities as in **b** for the 2D graphene superlattice specified in **c**.

tenths of an electron volt with appropriate perturbation and much larger than room temperature (Fig. 3b, Supplementary Discussion 5). We have also investigated the gap opening in 1D graphene superlattices with different values of length parameters (L and w). We find that, by changing these parameters, the anisotropy in the gap at the MB can also be controlled (Supplementary Discussion 5).

Due to the velocity renormalization near the Dirac point and the strong anisotropy in energy dispersion close to the MB, the type and the density of states (DOS) of

charge carriers vary drastically from those in graphene as one varies the Fermi energy (Fig. 4). As the Fermi level changes, the topology of the Fermi surface also exhibits a dramatic variation (Supplementary Discussion 6). For example, as the Fermi level increases from the energy at the Dirac point, the charge carriers of a 1D graphene superlattice fill electron orbits and show a linear increase in the DOS with slope larger than that of graphene; but above certain value, the DOS of electron orbits vanishes and charge carriers suddenly fill open orbits and hole pockets. When the Fermi level increases further, charge carriers are in purely open orbits and then the DOS of electron orbits starts to reappear and increases again (Fig. 4b). We expect that the Fermi level in a graphene superlattice can be tuned as in graphene by applying a gate voltage^{3,4,18,19}. Hence, by exploiting the various characteristics of charge carriers and the Fermi surface topology, one can manipulate a variety of physical properties dominated by the Fermi surface, such as conductance or magnetoresistance, significantly.

The anisotropic gap opening at the MB and the dramatic variation of the characters of charge carriers with the Fermi energy are also common in 2D graphene superlattices. The gap at the centres of the zone boundaries closes as in 1D graphene superlattice (Fig. 4c). However, the gap at the corners of the 2D MB also disappears. This behavior, which occurs in rectangular 2D graphene superlattices in general, has again its origin in the chiral nature of charge carriers in graphene (Supplementary Discussion 4). In a square 2D graphene superlattice, charge carriers are electrons, holes or a mixture of the two depending on the Fermi level (Fig. 4d). For general rectangular 2D graphene superlattices, charge carriers can also be in open orbits.

Here we have presented several novel physical properties of graphene superlattices with Kronig-Penney type 1D and muffin-tin type 2D potentials. Through additional calculations, we have confirmed that all the salient features of our findings are the same in sinusoidal or Gaussian types of graphene superlattices in general as well. The novel properties discovered in the present study thus should be of interest to the fundamental study and practical applications of graphene systems in general.

Finally, since the massless Dirac fermions in graphene superlattices have some features in common with high-energy relativistic particles propagating in anisotropic space like the anisotropy in the group velocity²⁹, interesting physics of the latter may also be investigated by table-top experiments based on our theoretical findings.

¹ Wallace, P. R. The band theory of graphite. *Phys. Rev.* **71**, 622–634 (1947).

² Novoselov, K. S. *et al.* Two dimensional atomic crystals. *Proc. Natl. Acad. Sci. USA.* **102**, 10451–10453 (2005).

³ Novoselov, K. S. *et al.* Two dimensional gas of massless Dirac fermions in graphene. *Nature* **438**, 197–200 (2005).

⁴ Zhang, Y., Tan, J. W., Stormer, H. L. & Kim, P. Experimental observation of the quantum hall effect and Berry's

- phase in graphene. *Nature* **438**, 201–204 (2005).
- ⁵ Berger, C. *et al.* Electronic confinement and coherence in patterned epitaxial graphene. *Science* **312**, 1191–1196 (2006).
 - ⁶ Geim, A. K. & Novoselov, K. S. The rise of graphene. *Nat. Mater.* **6**, 183–191 (2007).
 - ⁷ Son, Y.-W., Cohen, M. L. & Louie, S. G. Energy gaps in graphene nanoribbons. *Phys. Rev. Lett.* **97**, 216803 (2006).
 - ⁸ Son, Y.-W., Cohen, M. L. & Louie, S. G. Half-metallic graphene nanoribbons. *Nature* **444**, 347–349 (2006).
 - ⁹ Han, M. Y., Özyilmaz, B., Zhang, Y. & Kim, P. Energy band-gap engineering of graphene nanoribbons. *Phys. Rev. Lett.* **98**, 206805 (2007).
 - ¹⁰ Chen, Z., Lin, Y.-M., Rooks, M. J. & Avouris, P. Graphene nano-ribbon electronics. *Physica E* **40**, 228 (2007).
 - ¹¹ Esaki, L. & Tsu, R. Superlattice and negative differential conductivity in semiconductors. *IBM J. Res. Develop.* **14**, 61–65 (1970).
 - ¹² Tsu, R. *Superlattice to Nanoelectronics* (Elsevier, Oxford, UK, 2005).
 - ¹³ Cottam, M. G. & Tilley, D. R. *Introduction to Surface and Superlattice Excitations* (Cambridge Univ. Press, Cambridge, UK, 1989).
 - ¹⁴ Eigler, D. M. & Schweizer, E. K. Positioning single atoms with a scanning tunneling microscope. *Nature* **344**, 524–526 (1990).
 - ¹⁵ Crommie, M. F., Lutz, C. P. & Eigler, D. M. Confinement of electrons to quantum corrals on a metal surface. *Science* **262**, 218–220 (1993).
 - ¹⁶ Hiura, H. Tailoring graphite layers by scanning tunneling microscopy. *Appl. Surf. Sci.* **222**, 374–381 (2004).
 - ¹⁷ Williams, J. R., DiCarlo, L. & Marcus, C. M. Quantum hall effect in a gate-controlled p-n junction of graphene. *Science* **317**, 638–641 (2007).
 - ¹⁸ Huard, B. *et al.* Transport measurements across a tunable potential barrier in graphene. *Phys. Rev. Lett.* **98**, 236803 (2007).
 - ¹⁹ Özyilmaz, B. *et al.* Local gate control of electronic transport in graphene nanostructures. *Phys. Rev. Lett.* **99**, 166804 (2007).
 - ²⁰ Marchini, S., Günther, S. & Wintterlin, J. Scanning tunneling microscopy of graphene on ru(0001). *Phys. Rev. B* **76**, 075429 (2007).
 - ²¹ Vazquez de Parga, A. L. *et al.* Periodically rippled graphene: growth and spatially resolved electronic structure. *Phys. Rev. Lett.* **100**, 056807 (2008).
 - ²² Pan, Y. *et al.* Millimeter-scale, highly ordered single crystalline graphene grown on Ru (0001) surface. Preprint at <<http://arxiv.org/abs/0709.2858>> (2007).
 - ²³ Ando, T. & Nakanishi, T. Impurity scattering in carbon nanotubes - absence of back scattering. *J. Phys. Soc. Jpn.* **67**, 1704–1713 (1998).
 - ²⁴ Ando, T., Nakanishi, T. & Saito, R. Berry’s phase and absence of back scattering in carbon nanotubes. *J. Phys. Soc. Jpn.* **67**, 2857–2862 (1998).
 - ²⁵ DiVincenzo, D. P. & Mele, E. J. Self-consistent effective-mass theory for intralayer screening in graphite intercalation compounds. *Phys. Rev. B* **29**, 1685–1694 (1984).
 - ²⁶ McEuen, P. L., Bockrath, M., Cobden, D. H., Yoon, Y.-G. & Louie, S. G. Disorder, pseudospins, and backscattering in carbon nanotubes. *Phys. Rev. Lett.* **83**, 5098–5101 (1999).
 - ²⁷ Katsnelson, M. I., Novoselov, K. S. & Geim, A. K. Chiral tunneling and the Klein paradox in graphene. *Nature Phys.* **2**, 620–625 (2006).
 - ²⁸ Bai, C. & Zhang, X. Klein paradox and resonant tunneling in a graphene superlattice. *Phys. Rev. B* **76**, 075430 (2007).
 - ²⁹ Edwards, W. F. Special relativity in anisotropic space. *Am. J. Phys.* **31**, 482–489 (1963).

Acknowledgements C.-H.P. thanks J. D. Sau for fruitful discussions. This research was supported by the National Science Foundation (NSF) and by the Director, Office of Science, Office of Basic Energy Science, Division of Material Sciences and Engineering, US Department of Energy (DOE). Computational resources have been provided by the NSF at the National Partnership for Advanced Computational Infrastructure and by the DOE at the National Energy Research Scientific Computing Center. Y.-W.S. was supported by the Korea Science and Engineering Foundation grant funded by the Korea government (MOST).

Author Information The authors declare that they have no competing financial interests. Correspondence and requests for materials should be addressed to S.G.L. (e-mail: sglouie@berkeley.edu).

Supplementary Discussion 1 : Effective-Hamiltonian formalism

There are two carbon atoms per unit cell in graphene, forming two different sublattices, and hence the eigenstate of charge carriers in graphene can be represented by a two component basis vector. The Brillouin zone of graphene is a hexagon which has two inequivalent vertices, so-called the Dirac points, \mathbf{K} and \mathbf{K}' , that cannot be connected by reciprocal lattice vectors. In this work, we are considering eigenstates near \mathbf{K} only as discussed in the paper. The effective Hamiltonian for low-energy quasiparticles of graphene in this basis is given by

$$H_0(\mathbf{k}) = \hbar v_0 \begin{pmatrix} 0 & -ik_x - k_y \\ ik_x - k_y & 0 \end{pmatrix}, \quad (1)$$

where v_0 is the Fermi velocity and \mathbf{k} the small wavevector of the quasiparticle from the \mathbf{K} point in the Brillouin zone of graphene. The energy spectrum of this Hamiltonian is $E = s\hbar v_0 k$ where s is $+1$ or -1 for an eigenstate above or below the Dirac point energy which is defined to be the

energy zero, respectively. Eigenstates of this Hamiltonian is given by

$$\langle \mathbf{r} | s, \mathbf{k} \rangle = \frac{1}{\sqrt{2}} e^{i(\mathbf{K}+\mathbf{k}) \cdot \mathbf{r}} \begin{pmatrix} 1 \\ i s e^{i\theta_{\mathbf{k}}} \end{pmatrix}, \quad (2)$$

where $\theta_{\mathbf{k}}$ is the angle of vector \mathbf{k} with respect to the \hat{k}_x direction. Now, when an additional periodic potential $U(\mathbf{r})$ is applied to graphene, the scattering amplitude between states are given by

$$\langle s, \mathbf{k} | U(\mathbf{r}) | s', \mathbf{k}' \rangle = \sum_{\mathbf{G}} \frac{1}{2} (1 + s s' e^{-i\theta_{\mathbf{k}, \mathbf{k}-\mathbf{G}}}) U(\mathbf{G}) \delta_{\mathbf{k}', \mathbf{k}-\mathbf{G}}, \quad (3)$$

where \mathbf{G} and $U(\mathbf{G})$ are the reciprocal lattice vector and the corresponding Fourier component of the external periodic potential, respectively, and $\theta_{\mathbf{k}, \mathbf{k}-\mathbf{G}}$ the angle from $\mathbf{k} - \mathbf{G}$ to \mathbf{k} . The energy dispersions and eigenstates of the quasiparticles in a graphene superlattice are obtained non-perturbatively within the single-particle picture by solving the following set of linear equations:

$$(E - \varepsilon_{s, \mathbf{k}}) c(s, \mathbf{k}) = \sum_{s', \mathbf{G}} \frac{1}{2} (1 + s s' e^{-i\theta_{\mathbf{k}, \mathbf{k}-\mathbf{G}}}) U(\mathbf{G}) c(s', \mathbf{k} - \mathbf{G}), \quad (4)$$

where E is the superlattice energy eigenvalue and $\varepsilon_{s, \mathbf{k}} = s\hbar v_0 k$ the energy of the quasiparticles before applying the periodic potential. $c(s, \mathbf{k})$ and $c(s', \mathbf{k} - \mathbf{G})$ are the amplitudes of mixing among different unperturbed quasiparticle states.

Supplementary Discussion 2 : Velocity renormalization near the Dirac point from second order perturbation theory

When the external potential is weak, perturbative calculations can give results in good agreement with the full calculation and also in physically more intuitive forms. For pristine graphene, the group velocity of states near the Dirac point is parallel to \mathbf{k} and of constant magnitude (v_0). For a graphene superlattice, the renormalization in the component of the group velocity of quasiparticles parallel to the wavevector \mathbf{k} [$v_{\hat{k}} \equiv \mathbf{v}(\mathbf{k}) \cdot \hat{k}$] around the Dirac point can be obtained within second order perturbation approximation as

$$\frac{v_{\hat{k}} - v_0}{v_0} = - \sum_{\mathbf{G} \neq 0} \frac{2|U(\mathbf{G})|^2}{v_0^2 |\mathbf{G}|^2} \sin^2 \theta_{\mathbf{k}, \mathbf{G}}, \quad (5)$$

where $\theta_{\mathbf{k}, \mathbf{G}}$ is the angle from \mathbf{G} to \mathbf{k} . From Eq. (5), it is clear that for weak potentials, the velocity renormal-

ization grows as square of the amplitude of the external potential and $v_{\hat{k}}$ depends only on the direction of \mathbf{k} . Throughout this document, by weak potential we mean that the condition,

$$\frac{|U(\mathbf{G})|}{v_0 |\mathbf{G}|} \ll 1, \quad (6)$$

is satisfied for all the $U(\mathbf{G})$ components. In the absence of chirality of the states, the scattering matrix element [Eq. (3)] should be changed into

$$\langle s, \mathbf{k} | U(\mathbf{r}) | s', \mathbf{k}' \rangle = \sum_{\mathbf{G}} U(\mathbf{G}) \delta_{\mathbf{k}', \mathbf{k}-\mathbf{G}}. \quad (7)$$

Using Eq. (7), the similar quantity as in Eq. (5) for nonchiral massless Dirac fermions is now given by

$$\left(\frac{v_{\hat{k}} - v_0}{v_0} \right)_{\text{non-chiral}} = - \sum_{\mathbf{G} \neq 0} \frac{2|U(\mathbf{G})|^2}{v_0^2 |\mathbf{G}|^2}, \quad (8)$$

which is isotropic independent of the direction of \mathbf{k} . Comparing Eq. (5) and Eq. (8), the renormalization of group velocity in a one-dimensional (1D) superlattice for a fictitious graphene with states without chirality corresponds to the maximum renormalization in the corresponding 1D graphene superlattice. This trend agrees with the results from the full calculation when the potential is weak (Fig. 2 of paper).

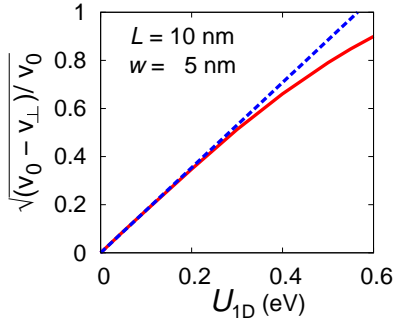


FIG. 5: (Supplementary Figure 1) **Dependence of the velocity renormalization on the amplitude of periodic potential in a 1D graphene superlattice.** Square root of the difference between the group velocity for state with \mathbf{k} along the direction perpendicular to the periodic direction of the potential (v_{\perp}) and the unrenormalized one (v_0) divided by v_0 versus the potential amplitude U_{1D} . Solid red line and dashed blue line are results of the full calculation and second order perturbation theory, respectively.

If Eq. (5) is applied to the Kronig-Penney type of 1D graphene superlattice periodic along the \hat{x} direction as discussed in the paper (Fig. 1b of paper),

$$\frac{v_{\hat{k}} - v_0}{v_0} = - \left\{ \frac{U_{1D}^2 L^2}{\pi^4 v_0^2} \sum_{n>0} \frac{1}{n^4} \sin^2 \left(\frac{\pi w}{L} n \right) \right\} \sin^2 \theta_{\mathbf{k}, \hat{x}}, \quad (9)$$

$$\begin{aligned} \frac{v_{\hat{k}} - v_0}{v_0} &\approx - \frac{U_{2D}^2 d^2}{4\pi^2 v_0^2} \left\{ \left(\frac{L_x}{L_y} \right)^2 J_1^2 \left(\frac{\pi d}{L_x} \right) \sin^2 \theta_{\mathbf{k}, \hat{x}} + \left(\frac{L_y}{L_x} \right)^2 J_1^2 \left(\frac{\pi d}{L_y} \right) \sin^2 \theta_{\mathbf{k}, \hat{y}} \right\} \\ &= - \frac{U_{2D}^2 d^2}{4\pi^2 v_0^2} \left\{ \left[\left(\frac{L_x}{L_y} \right)^2 J_1^2 \left(\frac{\pi d}{L_x} \right) - \left(\frac{L_y}{L_x} \right)^2 J_1^2 \left(\frac{\pi d}{L_y} \right) \right] \sin^2 \theta_{\mathbf{k}, \hat{x}} \right. \\ &\quad \left. + \left(\frac{L_y}{L_x} \right)^2 J_1^2 \left(\frac{\pi d}{L_y} \right) \right\} \end{aligned} \quad (11)$$

where the relation $\sin^2 \theta_{\mathbf{k}, \hat{y}} = 1 - \sin^2 \theta_{\mathbf{k}, \hat{x}}$ has been used in the second line. Now the group velocity $v_{\hat{k}}$ is renormalized in every direction. Equation (11) reproduces the sinusoidal variation of the velocity renormalization as well as the constant shift as obtained in the full calculation quite well when the potential is weak (Fig. 2b of paper).

Supplementary Discussion 3 : The magnitude and the component parallel to the wavevector \mathbf{k} of the group velocity

The component of the group velocity $v_{\hat{k}}$ parallel to the wavevector \mathbf{k} above is exactly equal to the absolute

value of the group velocity v_g when \mathbf{k} is at 0, 90, 180 or 270 degrees from the periodic direction of the applied potential and, when the applied potential is weak, is only slightly different from v_g at other angles (Supplementary Fig. 2).

where L is the spatial period of the potential, and U_{1D} and w are the height and the width of the rectangular potential barrier, respectively. Equation (9) is in good agreement with the full calculation when the potential is weak (Supplementary Fig. 1) and also shows sinusoidal behavior with respect to the polar angle of \mathbf{k} with respect to the periodic direction of the potential as well as the absence of renormalization for a particle moving across the potential barriers.

For the case of muffin-tin type of two-dimensional (2D) graphene superlattice (Fig. 1c of paper) periodic along both \hat{x} and \hat{y} directions, with periods L_x and L_y , respectively,

$$\frac{v_{\hat{k}} - v_0}{v_0} = - \frac{2\pi^2 U_{2D}^2 d^2}{v_0^2 L_x^2 L_y^2} \sum_{\mathbf{G} \neq 0} \frac{1}{G^4} J_1^2 \left(\frac{Gd}{2} \right) \sin^2 \theta_{\mathbf{k}, \mathbf{G}}, \quad (10)$$

where U_{2D} is the height of the circular potential barrier with diameter d and $\mathbf{G} = \left(\frac{2\pi}{L_x} m, \frac{2\pi}{L_y} n \right)$ the reciprocal lattice vector with integers m and n and $J_1(x)$ is the first order Bessel function of the first kind. When $L_x \approx L_y$ (as in Fig. 2b of paper), the dominant contribution in the sum comes from the terms with $|m| = 1, n = 0$ and $m = 0, |n| = 1$. Counting only these four terms,

value of the group velocity v_g when \mathbf{k} is at 0, 90, 180 or 270 degrees from the periodic direction of the applied potential and, when the applied potential is weak, is only slightly different from v_g at other angles (Supplementary Fig. 2).

Supplementary Discussion 4 : Band gap at the minizone boundary from degenerate perturbation theory

When the wavevector \mathbf{k} is on the minizone boundary (MB) of the 1D graphene superlattice, $k_x = \pm\pi/L$, two states $|s, \mathbf{k}\rangle$ and $|s, \mathbf{k} - (2\pi/L, 0)\rangle$ are degenerate before

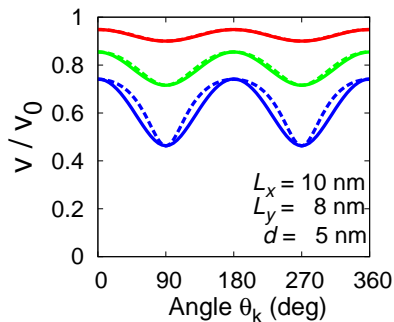


FIG. 6: (**Supplementary Figure 2**) **The magnitude and the component parallel to the wavevector \mathbf{k} of the renormalized group velocity in a 2D graphene superlattice.** The component of the group velocity parallel to the \mathbf{k} vector [$v_{\hat{k}} \equiv \mathbf{v}(\mathbf{k}) \cdot \hat{k}$ with \mathbf{k} measured from the Dirac point] of charge carriers in a 2D graphene superlattice (solid lines) and the absolute value of the group velocity (dashed lines) in units of the Fermi velocity in graphene (v_0) versus the angle ($\theta_{\mathbf{k}}$) of the \mathbf{k} -vector from the periodic potential direction \hat{x} . Red, green and blue lines correspond to the potential amplitude U_{2D} being 0.3 eV, 0.5 eV and 0.7 eV, respectively. Plotted quantities are obtained from the full calculation by solving Eq. (4).

$$H(\mathbf{k}) = \begin{pmatrix} \varepsilon_{s,\mathbf{k}} & U(2\pi/L) \\ \frac{1}{2}(1 + e^{i\theta_{\mathbf{k},\mathbf{k}-(2\pi/L,0)})} & \varepsilon_{s,\mathbf{k}-(2\pi/L,0)} \end{pmatrix}, \quad (12)$$

where $\varepsilon_{s,\mathbf{k}} = \varepsilon_{s,\mathbf{k}-(2\pi/L,0)} = s\hbar v_0 k$ is the energy of the charge carrier before the external potential is applied and $U(2\pi/L)$ the Fourier component of the periodic potential whose wavevector connects the two MBs at $k_x = \pm\pi/L$. The energy separate of the eigenvalues of Eq. (12) (i.e., the energy gap) is given by

$$\Delta E = 2 |U(2\pi/L) \sin \theta_{\mathbf{k},\hat{x}}|, \quad (13)$$

where $\theta_{\mathbf{k},\hat{x}}$ is the polar angle between \mathbf{k} and \hat{x} . Equation (13) clearly shows that the gap opening depends on \mathbf{k} and, in particular, is zero at the centre of the MB (Fig. 2 of paper), and that, as discussed in the paper, the maximum gap opening is proportional to the amplitude of the external potential in the weak potential regime.

If the chirality of the states in graphene is manually removed by using Eq. (7) for the scattering matrix element, the energy gap becomes

$$\Delta E_{\text{non-chiral}} = 2 |U(2\pi/L)|, \quad (14)$$

in which case the gap neither closes at the centre of the MB nor depends sensitively on the position along the MB in the weak potential limit (Fig. 2 of paper).

For a 2D rectangular graphene superlattice, in which the primitive translational lattice vectors are orthogonal, for the same reason as in the 1D case,

applying the periodic potential. The largest contribution to the energy eigenvalues at the MB comes from these two degenerate states. Scattering amplitude between these two states is given by Eq. (3). By choosing the origin at the centre of a potential barrier, we can make all the Fourier components of the periodic potential real without losing generality. Now the Hamiltonian for the two-state system is

the gap closes at the centres of MBs, i.e., when \mathbf{k} is at $(\pm\pi/L_x, 0)$ or $(0, \pm\pi/L_y)$. The more interesting case is the corner of the minizone, where the four degenerate states $|s, (\pi/L_x, \pi/L_y)\rangle$, $|s, (-\pi/L_x, \pi/L_y)\rangle$, $|s, (\pi/L_x, -\pi/L_y)\rangle$ and $|s, (-\pi/L_x, -\pi/L_y)\rangle$ mix strongly among themselves by the applied periodic potential. If we set up a similar matrix for this case like Eq. (12) for the 1D graphene superlattice, the energy eigenvalues of the matrix are

$$E = \varepsilon_{s,\mathbf{k}} \pm \sqrt{[U(2\pi/L_x, 0) \sin \theta_{\mathbf{k},\hat{x}}]^2 - [U(0, 2\pi/L_y) \cos \theta_{\mathbf{k},\hat{x}}]^2}, \quad (15)$$

where $\mathbf{k} = (\pi/L_x, \pi/L_y)$ is at the minizone corner and each eigenvalue is doubly degenerate. The energy spectrum given by Eq. (15) clearly shows that there is no gap at the minizone corner between the first and the second band (Fig. 4c of paper). This gap closure at the minizone corner is not obvious because a transition, which is not of a backscattering process, from one of the four \mathbf{k} points at the zone corners to another can occur in the 2D rectangular graphene superlattice. For example, the state $|s, (\pi/L_x, \pi/L_y)\rangle$ can mix with another state $|s, (-\pi/L_x, \pi/L_y)\rangle$ by the reciprocal lattice vector $\mathbf{G} = (2\pi/L_x, 0)$ but the two \mathbf{k} vectors are not anti-parallel. To understand the origin of the gap closure

at the minizone corner, we repeated a similar calculation for a 2D rectangular superlattice formed of a non-chiral

$$E_{\text{non-chiral}} = \varepsilon_{s,\mathbf{k}} + U(2\pi/L_x, 2\pi/L_y) \pm [U(2\pi/L_x, 0) - U(0, 2\pi/L_y)] ,$$

$$\varepsilon_{s,\mathbf{k}} - U(2\pi/L_x, 2\pi/L_y) \pm [U(2\pi/L_x, 0) + U(0, 2\pi/L_y)] . \quad (16)$$

According to Eq. (16), there is a finite energy gap between the first and the second band in general, other than in accidentally symmetric cases. Therefore, the gap closure at the minizone corner of a 2D rectangular graphene superlattice is a direct consequence of the chiral nature of the states in graphene.

Supplementary Discussion 5 : Dependence of the band gap at the minizone boundary on length parameters and broken particle-hole symmetry

For a Kronig-Penney type rectangular potential barrier 1D graphene superlattice, the energy gap at the MB can be expressed with Eq. (13) in terms of superlattice parameters as

$$\Delta E = \frac{2}{\pi} \left| U_{1D} \sin\left(\frac{\pi w}{L}\right) \sin \theta_{\mathbf{k},\hat{x}} \right| . \quad (17)$$

Thus, according to this simple degenerate perturbation theory result if the spatial period (L) becomes long for a constant barrier width (w) the gap should decrease, whereas if L is fixed and w is increased from zero, the gap should reach a maximum at $w = L/2$ and after that should decrease symmetrically. The former trend is observed in the full calculation (Supplementary Fig. 3a); however, the latter seems not to hold in the full calculation (Supplementary Fig. 3b). Moreover, the gap openings at the MB above and below the Dirac cone are different (Supplementary Fig. 3), which shows the limitation of the simple degenerate perturbation theory because the potential is not so weak and possesses higher Fourier components. One thing to note is that the energy dispersion for states above the energy of the Dirac point, including the gap opening, for a 1D Kronig-Penney type superlattice with width $w = w_0$ is identical with that of states below the energy of the Dirac point for width $w = L - w_0$ (Supplementary Fig. 3b, compare red and blue lines). This symmetry can be understood following a simple argument. If we start from a 1D Kronig-Penney superlattice with $w = w_0$ and then change w to be $w = L - w_0$ and at the same time invert the whole potential, the resulting periodic potential is identical to

system with linear energy dispersions. In this case, the energy eigenvalues are

the original one other than a constant shift which may be ignored. Inverting the potential is effectively the same as exchanging particles with holes.

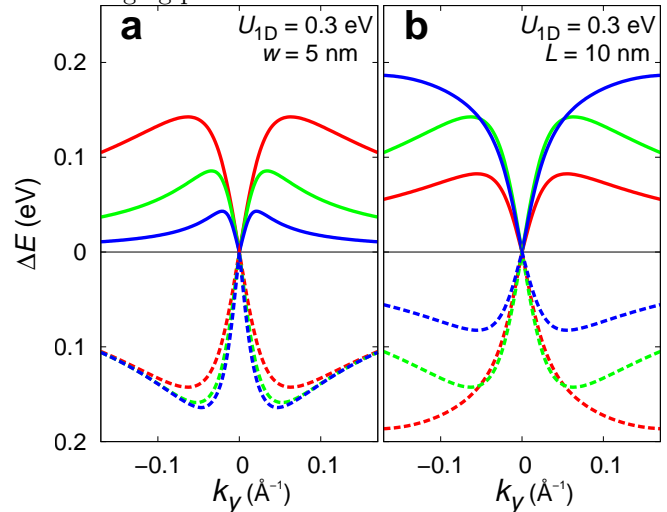


FIG. 7: (Supplementary Figure 3) Dependence of the energy gap at the minizone boundary on the length parameters of 1D graphene superlattice. **a**, The energy gap ΔE between the first and the second band at the minizone boundary versus k_y for charge carriers above (solid lines) and below (dashed lines) the energy at the Dirac point in a 1D graphene superlattice. Red, green and blue lines correspond to the spatial period (L) being 10 nm, 15 nm and 25 nm, respectively. **b**, Similar quantities as in **a**. Red, green and blue lines correspond to the potential barrier width (w) being 2.5 nm, 5 nm and 7.5 nm, respectively.

Supplementary Discussion 6 : Fermi surfaces

In 1D and 2D graphene superlattices, the topology as well as the shape of the Fermi surface varies significantly with the Fermi energy (Supplementary Figs. 4 and 5). This variation gives rise to a dramatic variation in the species and the density of states of charge carriers as a function of the position of the Fermi level (Fig. 5 of paper).

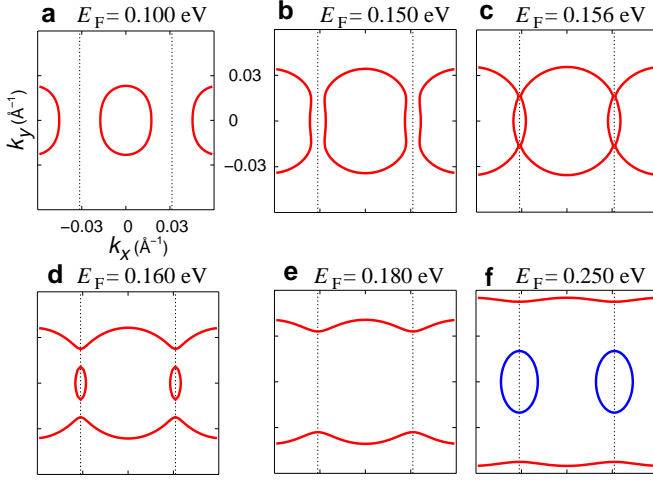


FIG. 8: (Supplementary Figure 4) Fermi surfaces of a 1D graphene superlattice. a-f, Fermi surfaces of 1D graphene superlattice with $U_{1D} = 0.3$ eV, $L = 10$ nm and $w = 5$ nm plotted in the repeated zone scheme for different values of the Fermi energy (E_F) with respect to that at the Dirac point. Dashed lines are minizone boundaries. Red and blue lines are parts coming from the first and the second band above the Dirac point energy, respectively.

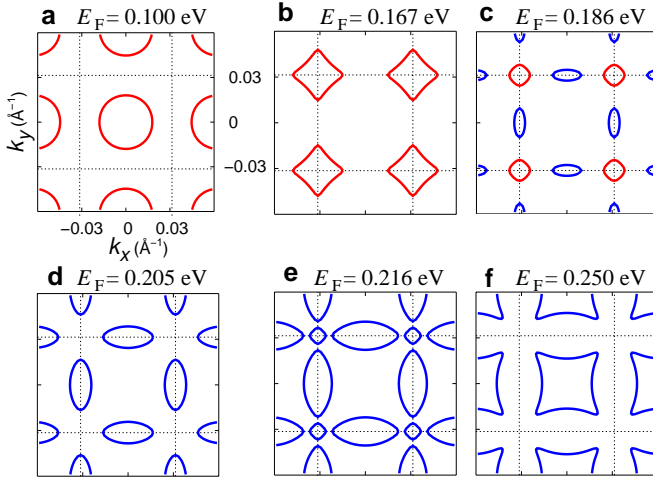


FIG. 9: (Supplementary Figure 5) Fermi surfaces of a 2D rectangular graphene superlattice. a-f, Fermi surfaces of a 2D rectangular graphene superlattice with $U_{2D} = 0.3$ eV, $L_x = L_y = 10$ nm and $d = 5$ nm plotted in the repeated zone scheme for different values of the Fermi energy (E_F) with respect to the Dirac point energy. Dashed lines are minizone boundaries. Red lines and blue line are parts coming from the first and the second band above the Dirac point energy, respectively.